Z. Angew. Math. Phys. (2018) 69:56

https://doi.org/10.1007/s00033-018-0947-4

Zeitschrift für angewandte
Mathematik und Physik ZAMP

Two-dimensional strain gradient damage modeling: a variational approach

Luca Placidi, Anil Misra and Emilio Barchiesi

Abstract. In this paper, we formulate a linear elastic second gradient isotropic two-dimensional continuum model accounting for irreversible damage. The failure is defined as the condition in which the damage parameter reaches 1, at least in one point of the domain. The quasi-static approximation is done, i.e., the kinetic energy is assumed to be negligible. In order to deal with dissipation, a damage dissipation term is considered in the deformation energy functional. The key goal of this paper is to apply a non-standard variational procedure to exploit the damage irreversibility argument. As a result, we derive not only the equilibrium equations but, notably, also the Karush–Kuhn–Tucker conditions. Finally, numerical simulations for exemplary problems are discussed as some constitutive parameters are varying, with the inclusion of a mesh-independence evidence. Element-free Galerkin method and moving least square shape functions have been employed.

Mathematics Subject Classification. 74R05.

Keywords. Strain gradient, 2D continua, Damage mechanics, Variational procedure, Karush–Kuhn–Tucker conditions.

1. Introduction

Material damaging and its consequent loss of material stiffness under loading can be viewed at various scales, ranging from the atomic to the material, with many intervening scales in the middle including molecular or crystal structures, grain boundaries and inter-granular layers, granular structures and so on [18,48,49,77,78]. At each scale, damage manifests in a unique and characteristic mechanism, from the formation and growth of atomic defects and dislocations in a crystal or molecule, passing through grain boundary sliding or rupture of inter-granular layers, to more coherent and cooperative phenomena at larger scales involving a large number of microstructural units [52,53,68–70,74]. For most complex material systems, the detailed description of these phenomena is beyond the reach of current analysis, regardless of the intense recent efforts at multiscale modeling. The multiscale methods connecting different scales have to rely on microstructure descriptions that are not readily available or easily conceived for complex material systems [17,28,39,71]. Multiscale simulations of macroscale mechanical behavior are not feasible or desirable for many materials that are suffused with complex, defective structures and interfaces of varying sizes. Furthermore, most materials offer significant challenges for atomistic modeling due to their complex composition and structure, since atomic models are practically infeasible at scales larger than the length of few hundred atoms. The difficulty of atomic models is not only confined to their high computational cost, but it is also due to the impossibility of specifying atomic structures for the myriad of material phases and interphases, including their defects.

For these reasons, continuum modeling is, arguably, the most feasible approach to damage modeling of complex material systems [19,21,22]. Many efforts, based upon continuum mechanics [5,12,55,56,58] and its various enhancements, have been reported in the literature dealing with damage modeling, as it has been discussed in an abridged form in authors' previous works [61,62,78]. The literature on regularized damage laws and the phase-field models [8,33,76] in which the regularisation is performed on damage variables has become quite intense in recent years. The reason for a regularization is due to the poor performances of local damage models when it comes to stress softening and, hence, the way to handle ultimate failure [57,58]. A regularization through the introduction of gradient of damage allows to overcome

Published online: 17 April 2018

the issues related to stress softening (localization, mesh-dependency) [46]. These models, in some cases, have been shown to converge to the Griffith model of brittle fracture, thus strengthening the choice of regularization through the damage variable [3,75]. However, the specification of natural boundary conditions corresponding to the damage variable may not always have a proper physical interpretation. A similar approach has been explored in the work of Forest [35], where the regularization procedure performed by Marigo and coworkers by means of the gradient of damage is applied to the micromorphic case. In [35], in fact, a variational procedure is shown and, therefore, a compatible set of boundary conditions has been derived. On the other hand, in the paper of Peerlings et al. [54] no variational procedure is used. Accordingly, in their case [54], no external double forces nor external vertex forces are considered.

These discussions clearly show that damage modeling of materials and structures remains a challenging problem that deserves a treatment from a generalized continuum approach founded upon a robust variational formulation [2,6,14,20,23,26,30,32,60]. The advantages of such an approach are the clear identification of the damage evolution behavior together with the definition of relevant governing equations and boundary conditions.

The goal of this paper is to develop, for the first time, a non-standard variational procedure aimed to obtain simultaneously the second gradient equilibrium equations and the Karush–Kuhn–Tucker conditions for the present 2D case. This is achieved by generalizing the results that have been obtained previously, by the first author, for the 1D axial case for damage [61] and plasticity [62]. The derived formulation is used to establish a numerical approach for showing the evolution of damage in a rectangular plate. Element-free Galerkin (EFG) method has been used [10,45], and the domain has been discretized into a set of nodes with Moving Least Square (MLS) shape functions (see also [77,78]). This numerical scheme could also be implemented by the use of higher continuity shape functions [11,15,16,40,41]. No extrinsic defect is introduced in the plate, and the damage is shown to evolve from the specified boundary conditions.

We observe that it could be of interest to generalize these results to the modeling of carbon nanotubes [4], of bones [7,37,42], of cementitious or of granular materials [50,70] (where it is also possible to consider the anisotropy induced from damage [51]) for quasi-static or for the dynamic cases [13,59,72]. Besides, this approach could be particularly significant for modeling 2D structures such as pantographic sheets or fiber textile composites and elastic nets [27,38,43,67,73]. For these structures, the second gradient or micromorphic continuum models, based upon a variational approach, could be particularly useful not only for modeling their unique deformation behaviors, that include the formation of finite boundary layers, but, more importantly, for establishing unambiguous governing equations, boundary conditions and evolution relationships in the irreversible damage context. It is worth to be noted that even for the purely elastic case, where no damage nor gradient of damage is necessary, deformation behaviors with boundary layers are routinely observed [34,44].

2. Formulation of the problem

2.1. Preliminary definitions

The body $\mathcal{B}$ is modeled in the reference configuration as, for the sake of simplicity, a 2-dimensional continuum and each one of its body points is determined by means of the coordinates X in some frame of reference. The set of kinematical descriptors for such a model does not contain, as usual, the displacement field $u = u(X,t)$ only, but it also contains the damage field $\omega = \omega(X,t)$. The damage state of a material point X is therefore characterized, at time t and again for the sake of simplicity, by a scalar internal variable ω, that is assumed to be within the range $[0,1]$. The cases $\omega = 0$ and $\omega = 1$ correspond to the undamaged state and to failure, respectively. Even if, for a certain ω, the behavior is assumed to be elastic, since ω evolves in time, the behavior is inelastic and is defined by an internal deformation energy density functional U, which is a real function of the displacement and damage fields, i.e., $U(u(\cdot),\omega(\cdot))$.

Let us perform the quasi-static approximation, that is equivalent to say that inertia, i.e., the kinetic energy, is negligible. We remark that a damaged state with $\omega > 0$ corresponds, in the real material, to a certain number of missing atomic bonds. We assume the material to be not self-healing and, hence, ω is assumed to be a non-decreasing function of time. This implies that the transition from undamaged to damaged states is irreversible and, roughly speaking, the total deformation energy is dissipated as far as the damage increases its value. In order to handle dissipation, one could employ a Rayleigh dissipation functional or, simply, consider a dissipation term in U, in the same way as Marigo and his coworkers [5,12,55,56,58] do in their approach to damage mechanics. With this different approach, the procedure to find the evolution of the fundamental kinematical fields from the total deformation energy functional, because of the monotonicity assumption on ω, is not the standard one, in which the first variation of the total deformation energy is assumed to vanish [9,24,25,29,31,47,63]. One has instead to resort to a different variational principle [61,62]. We shall address this issue later on in Sect. 2.3.

If we look at the damaged material as a microstructured material, i.e., damage gives a microstructure, it is meaningful to let the internal deformation energy density depend upon the second gradient of the displacement. Thus, because of objectivity, the deformation density energy functional is assumed to be a function of the strain tensor $G = \left(F^T F - I\right)/2$, of its gradient ∇G and of the damage ω, i.e., $U = U\left(G, \nabla G, \omega\right)$. Here, $F = \nabla\chi$, where $\chi = X + u$ is the placement function, F^T is the transpose of F, and ∇ is the gradient operator. For the small displacement approximation that is dealt in this paper, the strain tensor G is assumed to be equal to $E = \mathrm{Sym}\left(H\right)$, the symmetric part of the displacement gradient $H = \nabla u$.

2.2. Total deformation energy functional

The total deformation energy functional $\mathcal{E}\left(u, \omega\right)$ depends on the displacement u and the damage ω:

$$\mathcal{E}\left(u,\omega\right) = \int\limits_{\mathcal{B}} \left[U\left(G, \nabla G, \omega\right) - b^{\mathrm{ext}} \cdot u - m^{\mathrm{ext}} \cdot \nabla u\right] \mathrm{d}A + \tag{1}$$

$$- \int\limits_{\partial\mathcal{B}} \left[t^{\mathrm{ext}} \cdot u + \tau^{\mathrm{ext}} \cdot \left[\left(\nabla u\right) n\right]\right] ds - \int\limits_{[\partial\partial\mathcal{B}]} f^{\mathrm{ext}} \cdot u. \tag{2}$$

In (1–2), n is the unit external normal; the dot $(\cdot)$ indicates the scalar product between vectors or tensors; b^{ext} and m^{ext} are the external body force and double force (per unit area), respectively; t^{ext} and τ^{ext} are the external force and double force (per unit length), respectively; f^{ext} is the external concentrated force which is applied on the vertices $[\partial\partial\mathcal{B}]$. Thus, the last integral in (2) is the sum of the external works accomplished by the external concentrated forces applied at the vertices. Besides,

$$\partial\mathcal{B} = \bigcup_{c=1}^{m} \Sigma_c, \qquad [\partial\partial\mathcal{B}] = \bigcup_{c=1}^{m} \mathcal{V}_c.$$

The boundary $\partial\mathcal{B}$ is the union of m regular parts Σ_c (with $c = 1, \ldots, m$) and the so-called boundary of the boundary $[\partial\partial\mathcal{B}]$ is the union of the corresponding m vertex-points $\mathcal{V}_c$ with coordinates X^c.

2.3. Variational principle

In order to get governing equations for this model, we resort to the variational principle thoroughly presented in [61,62], where the case of one-dimensional bodies was considered. Thus, we assume that the motion $u\left(X,t\right)$ and $\omega\left(X,t\right)$ verifies the condition

$$\delta\mathcal{E}\left(u, \omega, \dot{u}, \dot{\omega}\right) \leq \delta\mathcal{E}\left(u, \omega, \upsilon, \beta\right), \qquad \forall\upsilon,\ \forall\beta \geq 0, \tag{3}$$

where υ and β are compatible virtual velocities and dots represent derivation with respect to time. We remark that in the present quasi-static case the time can be substituted by any other parameter, e.g., by a loading parameter. Besides, the formulation that is given in (3) is a principle and no prove will be here furnished. Nevertheless, we will provide in the following mathematical derivations of this principle that could be used to achieve those numerical simulations that are necessary for its scientific validation. First, we shall estimate the first variation

$$\delta\mathcal{E}\left(u,\omega,\delta u,\delta\omega\right) \tag{4}$$

$$= \int_{\mathcal{B}} \left[\frac{\partial U}{\partial G_{ij}}\delta G_{ij} + \frac{\partial U}{\partial G_{ij,h}}\delta G_{ij,h} + \frac{\partial U}{\partial \omega}\delta\omega - b_i^{\text{ext}}\delta u_i - m_{ij}^{\text{ext}}\delta u_{i,j} \right] + \tag{5}$$

$$- \int_{\partial\mathcal{B}} \left[t_i^{\text{ext}}\delta u_i + \tau_i^{\text{ext}}\delta u_{i,j}n_j \right] - \int_{[\partial\partial\mathcal{B}]} \left[f_i^{\text{ext}}\delta u_i \right]. \tag{6}$$

Integrating by parts and assuming the small displacement approximation, we get

$$\delta\mathcal{E} = -\int_{\mathcal{B}} \left\{ \delta u_i \left[\left(\sigma_{ij} - T_{ijh,h}\right)_{,j} + b_i^{\text{ext}} - m_{ij,j}^{\text{ext}} \right] + \delta\omega\frac{\partial U}{\partial\omega} \right\} \tag{7}$$

$$+ \int_{\partial\mathcal{B}} \left[\delta u_i \left(t_i - t_i^{\text{ext}} - m_{ij}^{\text{ext}}n_j \right) + \delta u_{i,j}n_j \left(\tau_i - \tau_i^{\text{ext}} \right) \right] \tag{8}$$

$$+ \int_{[\partial\partial\mathcal{B}]} \delta u_i \left(f_i - f_i^{\text{ext}} \right), \tag{9}$$

where the so-called contact force t, contact double force τ and contact vertex force f have been defined as

$$t_i = \left(\sigma_{ij} - T_{ijh,h}\right)n_j - P_{ka}\left(T_{ihj}P_{ah}n_j\right)_{,k},\ \tau_i = T_{ijk}n_jn_k,\ f_i = T_{ihj}V_{hj}, \tag{10}$$

where P is the tangential projector operator ($P_{ij} = \delta_{ij} - n_in_j$), V is the vertex operator

$$V_{hj} = \nu_h^l n_j^l + \nu_h^r n_j^r, \tag{11}$$

ν is the external tangent unit vector. The superscripts l and r, respectively, refer, roughly speaking, to the left and right side of a certain vertex-point $\mathcal{V}_c$. The stress tensor σ and the hyper stress tensor T are defined as

$$\sigma_{ij} = \frac{\partial U}{\partial G_{ij}}, \qquad T_{ijh} = \frac{\partial U}{\partial G_{ij,h}}. \tag{12}$$

It is worth to be noted that, by looking at the first addend of (8), the external part $t^{\text{ext}} + m^{\text{ext}}n$ of the dual of the virtual displacement δu is not equal to the external force per unit length t^{ext}.

2.3.1. Reduction to the standard variational principle. Let us verify that the variational principle expressed in (3) reduces to the usual one, i.e., $\delta\mathcal{E} = 0$ for arbitrary variations δu, when no variation $\delta\omega$ is considered. Namely, we want to check that

$$\delta\mathcal{E}\left(u,\omega,\delta u,0\right) = 0. \tag{13}$$

Let us choose $\upsilon = \dot{u} + \overline{\upsilon}$, with arbitrary $\overline{\upsilon}$, and $\beta = \dot{\omega}$ in (3). We get

$$\delta\mathcal{E}\left(u,\omega,\dot{u},\dot{\omega}\right) \leq \delta\mathcal{E}\left(u,\omega,\dot{u}+\overline{\upsilon},\dot{\omega}\right). \tag{14}$$

Let us choose $\upsilon = \dot{u} - \overline{\upsilon}$, with arbitrary $\overline{\upsilon}$, and $\beta = \dot{\omega}$ in (3). We get

$$\delta\mathcal{E}\left(u,\omega,\dot{u},\dot{\omega}\right) \leq \delta\mathcal{E}\left(u,\omega,\dot{u}-\overline{\upsilon},\dot{\omega}\right). \tag{15}$$

Since the first variation of a functional is a linear function of the admissible variations, (14) implies

$$\delta\mathcal{E}\left(u,\omega,\overline{v},0\right)\geq 0, \tag{16}$$

and (15) implies

$$\delta\mathcal{E}\left(u,\omega,\overline{v},0\right)\leq 0. \tag{17}$$

Combining (16) and (17) we obtain

$$\delta\mathcal{E}\left(u,\omega,\bar{v},0\right)=0 \quad \forall\overline{v}. \tag{18}$$

By applying the localization theorem to (18), we get

$$\left(\sigma_{ij}-T_{ijh,h}\right)_{,j}+b_i^{\text{ext}}-m_{ij,j}^{\text{ext}}=0 \quad \forall X\in\mathcal{B}. \tag{19}$$

For those points of $\partial\mathcal{B}\backslash[\partial\partial\mathcal{B}]$ where we do not have the kinematical constraints $\delta u_i=0$, we have the natural boundary conditions $t_i-t_i^{\text{ext}}-m_{ij}^{\text{ext}}n_j=0$. For those points of the $\partial\mathcal{B}\backslash[\partial\partial\mathcal{B}]$ where we do not have the kinematical constraints $\delta u_{i,j}n_j=0$, we have the natural boundary conditions $\tau_i-\tau_i^{\text{ext}}=0$. Finally, for those points of $[\partial\partial\mathcal{B}]$ where we do not have the kinematical constraints, $\delta u_i=0$, we have the natural boundary conditions $f_i-f_i^{\text{ext}}=0$.

2.3.2. Exploiting the non-standard argument. Let us choose $\upsilon=\dot{u}$ and $\beta=0$ in (3). We get

$$\delta\mathcal{E}\left(u,\omega,\dot{u},\dot{\omega}\right)\leq\delta\mathcal{E}\left(u,\omega,\dot{u},0\right). \tag{20}$$

Let us choose $\upsilon=\dot{u}$ and $\beta=2\dot{\omega}$ in (3). We get

$$\delta\mathcal{E}\left(u,\omega,\dot{u},\dot{\omega}\right)\leq\delta\mathcal{E}\left(u,\omega,\dot{u},2\dot{\omega}\right). \tag{21}$$

Since the first variation of a functional is a linear function of the admissible variations, (20) implies

$$\delta\mathcal{E}\left(u,\omega,0,\dot{\omega}\right)\leq 0, \tag{22}$$

and (21) implies

$$\delta\mathcal{E}\left(u,\omega,0,\dot{\omega}\right)\geq 0. \tag{23}$$

Combining (22) and (23), we obtain

$$\delta\mathcal{E}\left(u,\omega,0,\dot{\omega}\right)=0 \tag{24}$$

and, therefore, from (7)–(9) and (24)

$$\int_{\mathcal{B}}\frac{\partial U}{\partial\omega}\dot{\omega}=0. \tag{25}$$

Let us choose $\upsilon=\dot{u}$ in (3). We get

$$\delta\mathcal{E}\left(u,\omega,\dot{u},\dot{\omega}\right)\leq\delta\mathcal{E}\left(u,\omega,\dot{u},\beta\right)\ \forall\beta\geq 0. \tag{26}$$

By linearity, we easily see that

$$\delta\mathcal{E}\left(u,\omega,0,\beta-\dot{\omega}\right)\geq 0\ \forall\beta\geq 0. \tag{27}$$

Reminding (24) and using again linearity, (27) reads as

$$\delta\mathcal{E}\left(u,\omega,0,\beta\right)\geq 0\ \forall\beta\geq 0$$

and, therefore,

$$\int_{\mathcal{B}}\frac{\partial U}{\partial\omega}\beta\geq 0\ \forall\beta\geq 0. \tag{28}$$

Now, let $\Omega_\gamma(\overline{X})\subset\mathbb{R}^2$ a family, parameterized over $\gamma\in\mathbb{R}^+$, of bounded neighborhoods of $\overline{X}\in\mathcal{B}$, such that diam $\Omega_\gamma(\overline{X})=\gamma$. Besides, let $\beta_\gamma:\ \mathcal{B}\to\mathbb{R}^+$ a family of functions, parameterized over $\gamma\in\mathbb{R}^+$, defined as

$$\beta_\gamma(X)=\begin{cases}0 & \text{if } X\notin\Omega_\gamma(\overline{X})\\ 1 & \text{if } X\in\Omega_\gamma(\overline{X}).\end{cases} \tag{29}$$

Clearly, for each $\gamma \in \mathbb{R}^+$, β_γ defined in (29) fulfills the positive definiteness required to β in (28). Hence, we have

$$\int_{\mathcal{B}} \frac{\partial U}{\partial \omega} \beta_\gamma \geq 0, \ \gamma \in \mathbb{R}^+$$

and, letting $\gamma \to 0^+$, we finally get

$$\frac{\partial U}{\partial \omega} \geq 0 \ \forall X \in \mathcal{B}. \tag{30}$$

Since by hypothesis $\dot{\omega} \geq 0$ and by (30) $\frac{\partial U}{\partial \omega} \geq 0 \ \forall X \in \mathcal{B}$, in order to fulfill the relation (25) $\int_{\mathcal{B}} \frac{\partial U}{\partial \omega} \dot{\omega} = 0$, we get that $\frac{\partial U}{\partial \omega}$ and/or $\dot{\omega}$ must vanish for each point X of $\mathcal{B}$ and time t:

$$\frac{\partial U}{\partial \omega} \dot{\omega} = 0. \tag{31}$$

Thus, we have derived the so-called Karush–Kuhn–Tucker (KKT) conditions for damage mechanics simply from the variational principle given in (3).

2.4. Consequence of using a 2D isotropic quadratic internal deformation energy density functional accounting for damage

A general form of the elastic part U_e of the internal deformation energy density functional U of a 3D isotropic second gradient elastic material is provided in [47]. We have

$$\begin{aligned} U_e\left(G, \nabla G\right) = & \frac{\lambda}{2} G_{ii} G_{jj} + \mu G_{ij} G_{ij} + 4\alpha_1 G_{ii,j} G_{jh,h} + \alpha_2 G_{ii,j} G_{kk,j} \\ & + 4\alpha_3 G_{ij,i} G_{kj,k} + 2\alpha_4 G_{ij,k} G_{ij,k} + 4\alpha_5 G_{ij,k} G_{ik,j}, \end{aligned} \tag{32}$$

where λ , μ, α_1, α_2, α_3, α_4, $\alpha_5 \in \mathbb{R}$ are independent parameters; λ and μ are referred to as the Lamé parameters (that can be easily related to the Young modulus Y and to the Poisson ratio ν) and this choice is clear by looking at (32) without (additive) strain gradient terms. The parameters λ, μ, α_i do not depend upon the strain tensor and/or its gradient while, nevertheless, they are functions of $X \in \mathcal{B}$ and t, i.e., they are scalar fields depending upon time.

When the specialization of (32) to the plane strain case ($u_{1,3} = u_{2,3} = u_3 = 0$) is considered, we have

$$\begin{aligned} U_e\left(G, \nabla G\right) = & 2\mu \ {G_{12}}^2 + \lambda \ G_{11} G_{22} + \left(\frac{\lambda}{2} + \mu\right) \ {G_{11}}^2 + \left(\frac{\lambda}{2} + \mu\right) \ {G_{22}}^2 \\ & + \left(\frac{3A}{2} - B + C + 2D\right) \ G_{11,2}^2 + \left(-\frac{A}{2} - \frac{B}{2} + C + 2D\right) \ G_{11,2} G_{22,2} + \\ & + \left(-4A + 2B - 4D\right) \ G_{11,2} G_{12,1} + 2A \ \left({G_{12,1}}^2 + {G_{12,2}}^2\right) \\ & + \left(A + B - 2C\right) \ G_{11,1} G_{12,2} + \left(\frac{3A}{2} - B + C + 2D\right) \ {G_{22,1}}^2 \\ & + \left(-\frac{A}{2} - \frac{B}{2} + C + 2D\right) \ G_{11,1} G_{22,1} + \left(-4A + 2B - 4D\right) \ G_{12,2} G_{22,1} \\ & + \left(A + B - 2C\right) \ G_{12,1} G_{22,2} + \frac{B}{2} \ \left({G_{11,1}}^2 + {G_{22,2}}^2\right), \end{aligned} \tag{33}$$

that is equivalent to that used in [63,66] and where

$$\begin{pmatrix} A \\ B \\ C \\ D \end{pmatrix} = \begin{pmatrix} 0 & 0 & 2 & 2 & 2 \\ 8 & 2 & 8 & 4 & 8 \\ 2 & 1 & 1 & 3 & 5 \\ 3 & 1 & 2 & 0 & 0 \end{pmatrix} \begin{pmatrix} \alpha_1 \\ \alpha_2 \\ \alpha_3 \\ \alpha_4 \\ \alpha_5 \end{pmatrix}, \tag{34}$$

We now include the damage ω, according with [61], by adding a quadratic damage-term in the internal energy

$$U_e\left(G, \nabla G\right) \rightarrow U\left(G, \nabla G, \omega\right) = U_e\left(G, \nabla G\right) + \frac{k}{2}\omega^2, \tag{35}$$

where k is the resistance to damage and, by assuming an explicit dependence of the parameters $\lambda, \mu, \alpha_1, \alpha_2, \alpha_3, \alpha_4, \alpha_5$ upon the damage ω, we have

$$\lambda = \lambda_0\left(1-\omega\right), \qquad \mu = \mu_0\left(1-\omega\right) \tag{36}$$

$$\alpha_i = \alpha_i^0\left(1+n\omega\right), \ n \in \mathbb{R}, \ i = 1,2,3,4,5. \tag{37}$$

Defining from (34) the undamaged second gradient 2D elastic coefficients,

$$\begin{pmatrix} A_0 \\ B_0 \\ C_0 \\ D_0 \end{pmatrix} = \begin{pmatrix} 0 & 0 & 2 & 2 & 2 \\ 8 & 2 & 8 & 4 & 8 \\ 2 & 1 & 1 & 3 & 5 \\ 3 & 1 & 2 & 0 & 0 \end{pmatrix} \begin{pmatrix} \alpha_1^0 \\ \alpha_2^0 \\ \alpha_3^0 \\ \alpha_4^0 \\ \alpha_5^0 \end{pmatrix},$$

when the specialization of (32) to the plane strain case is considered, we have that $(37)_3$ reads as

$$\begin{pmatrix} A \\ B \\ C \\ D \end{pmatrix} = (1+n\omega) \begin{pmatrix} A_0 \\ B_0 \\ C_0 \\ D_0 \end{pmatrix}. \tag{38}$$

It is worth to be noted that in the general $2D$ case one might directly assume (38) instead of (37). In (37), the parameter n is a weight for the damage which ranges from -1 to infinite, i.e., $n \in [-1, +\infty)$. The case $n = -1$ is related to fracture because in this case no elastic energy can be accumulated in the completely cracked region [65]. Besides, $n = 0$ means that coefficients α_i's are independent of ω. This corresponds to the case where the damage does not affect the characteristic length scales of the material. The case of large value of the parameter n is connected to diffused damaged materials, and it is associated with an increase of material characteristic length while the overall material undergoes softening. The functions relating the second gradient coefficients with the damage parameter are based on some constitutive assumptions that should be determined by experiments that need to be conceived. However, the second gradient coefficients, as well as damage, are a measure of the microstructure.

For example, let us assume that in an initially homogeneous material with no microstructure, some distributed defects are added as the material is subjected to loading. We therefore can interpret the new material not only as a damaged one (of course) but also as a material with microstructures. For example, it is clear that the first homogeneous material does not have a dynamic dispersive behavior and the second damaged (or microstructured) one has a dispersive behavior at least for some frequency range. The correlation between microstructured and strain gradient materials is widely accepted. Thus, damage can be interpreted as an amplifier of the microstructure and, in our opinion, it is reasonable that, at least in some cases, second gradient coefficients increase with damage and, accordingly, we consider $n > 0$. The cases in which $n < 0$ indicates a localization into fracture, that deserves as well to be studied. We will nevertheless show, in Figs. 3 and 5, simulations for selected values of the cases $n > 0$, $n = 0$ and $n < 0$.

The above formulation precludes any elastic phase. However, the dissipation energy could be reformulated in a manner which includes an elastic phase by adding in (35) a linear term in ω, as it is shown in the paper [62] dealing with the 1D case. Besides, in the formulation (36) only stress softening process is included. It would be possible to have a stress hardening by incorporating some induced anisotropic effects which are, however, excluded by the present isotropic formulation.

We remark that, due to (37) or to (38), the model presented so far in this paper does not apply to failure. Indeed, for $\omega = 1$ (and, given that U is continuous with respect to ω, the forthcoming statement is true in a left neighborhood of $\omega = 1$) the deformation energy functional U is not necessarily positive definite. It is for this reason that, in this paper, all numerical simulations are stopped one step before the failure.

The explicit form, with respect to damage, of the density of the deformation internal energy (35) is derived from (33) and (38).

Plugging such an explicit form in (19) and using (12), in the case of no external distributed actions, i.e., in the case $b^{\text{ext}} = m^{\text{ext}} = 0$, we get the two PDEs of the problem.

In Sect. 2.3, we have proved that, for each point X of $\mathcal{B}$ and time t, $\frac{\partial U}{\partial \omega}$ or/and $\dot{\omega}$ must vanish. From the condition (31) we get

$$\begin{aligned}\omega(X,t) = &\frac{\lambda_0 + 2\mu_0}{k}\left(u_{1,1}^2 + u_{2,2}^2\right) + 2\frac{\mu_0}{k}u_{1,2}u_{2,1} + 2\frac{\lambda_0}{k}u_{1,1}u_{2,2}\\ &+\frac{\mu_0}{k}\left(u_{1,2}^2 + u_{1,1}^2\right) - 2n\frac{D_0}{k}\left(u_{1,11}u_{2,12} + u_{2,22}u_{1,12}\right)\\ &-n\frac{A_0}{k}\left(u_{1,22}^2 + u_{2,11}^2\right) - n\frac{B_0}{k}\left(u_{1,11}^2 + u_{2,22}^2\right) - n\frac{C_0}{k}\left(u_{1,12}^2 + u_{2,12}^2\right) +\\ &-n\frac{B_0 - C_0 + A_0}{k}\left(u_{1,11}u_{1,22} + u_{2,11}u_{2,22}\right) +\\ &-2n\frac{B_0 - A_0 - D_0}{k}\left(u_{1,12}u_{2,11} + u_{1,22}u_{2,12}\right). \end{aligned} \tag{39}$$

If $\omega(X,t)$ computed by using (39) is such that $\dot{\omega} < 0$ then $\dot{\omega} = 0$. This provides a useful tool to numerically compute the field $\omega(X,t)$. Indeed, fixed $X \in \mathcal{B}$ and for each time step t, the following condition must be verified

$$\omega(X,t) \geq \omega(X, t - \Delta t).$$

If this is not the case, then

$$\omega(X,t) = \omega(X, t - \Delta t).$$

3. Numerical examples

In this section, we study the case of a rectangular body (see Fig. 1 (top)) with sides of length L and $2l$. This choice is motivated by the fact that since all the boundaries are straight, the external normals (for each side) do not depend on the space-coordinate X. Therefore, boundary conditions are simplified. Moreover, the set $[\partial\partial\mathcal{B}]$ of the vertices is non-empty. Boundary conditions are shown in Fig. 1 (bottom) for tension (bottom-left) and shear (bottom-right) and derived in the following subsection.

3.1. Side and vertex boundary conditions

For side S1 (with normal unit vector $n_i = -\delta_{i1}$), we have essential boundary conditions for displacement and natural boundary conditions for normal displacement gradient:

$$\begin{aligned}&u_1(0,y) = 0,\ u_2(0,y) = 0,,\ \forall y \in [-l,l]\\ &\tau_i(0,y) = \tau_i^{\text{ext},S1}(y) = 0\ \forall y \in [-l,l],\ i = 1,2,\end{aligned} \tag{40}$$

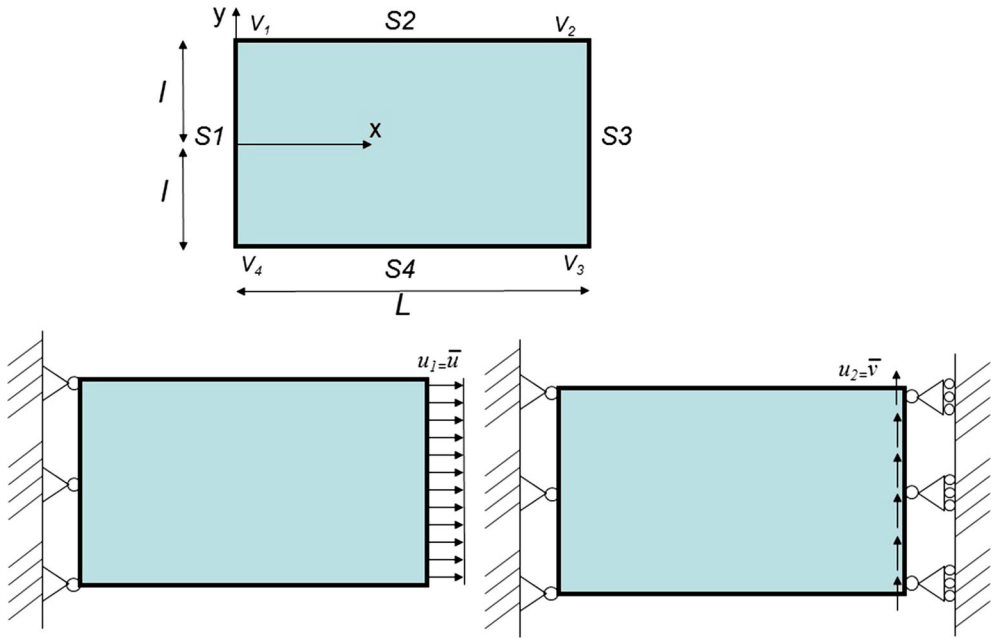

FIG. 1. Definition of the frame of reference and classification of the sides and of the vertices of the body $\mathcal{B}$ (top). External forces and constraints in the tension (bottom-left) and shear (bottom-right) cases

For side S2 (with normal unit vector $n_i = \delta_{i2}$), we have natural conditions for both displacement and normal displacement gradient,

$$t_i(x,l) = t_i^{\text{ext},S2}(x) = 0,\ \forall x \in [0,L],\ i = 1,2,$$
$$\tau_i(x,l) = \tau_i^{\text{ext},S2}(x) = 0,\ \forall x \in [0,L],\ i = 1,2, \tag{41}$$

For side S3 (with normal unit vector $n_i = \delta_{i1}$), we have natural boundary conditions for normal displacement gradient

$$\tau_i(L,y) = \tau_i^{\text{ext},S3}(y) = 0,\ \forall y \in [-l,l],\ i = 1,2, \tag{42}$$

and for the tension case an essential boundary condition for horizontal displacement and a natural boundary condition for vertical displacement,

$$u_1(L,y) = \overline{u},\ t_2(L,y) = t_2^{\text{ext},S3}(y) = 0,\ \forall y \in [-l,l], \tag{43}$$

while for the shear case an essential boundary condition for vertical displacement and a natural boundary condition for horizontal displacement,

$$u_2(L,y) = \overline{v},\ t_1(L,y) = t_1^{\text{ext},S3}(y) = 0,\ \forall y \in [-l,l]. \tag{44}$$

For side S4 (with normal unit vector $n_i = -\delta_{i2}$), we have natural boundary conditions for both displacement and normal displacement gradient,

$$t_i(x,-l) = t_i^{\text{ext},S4}(x),\ \tau_i(x,-l) = \tau_i^{\text{ext},S4}(x),\ \forall x \in [0,L],\ i = 1,2. \tag{45}$$

As far as vertices are concerned, we consider only natural boundary conditions, since essential ones have been already analyzed. Vertices V_2 and V_3 do have natural boundary conditions in the vertical direction for the tension case,

$$f_2^{V_2} = f_2^{\text{ext},V_2} = 0, \quad f_2^{V_3} = f_2^{\text{ext},V_3} = 0, \tag{46}$$

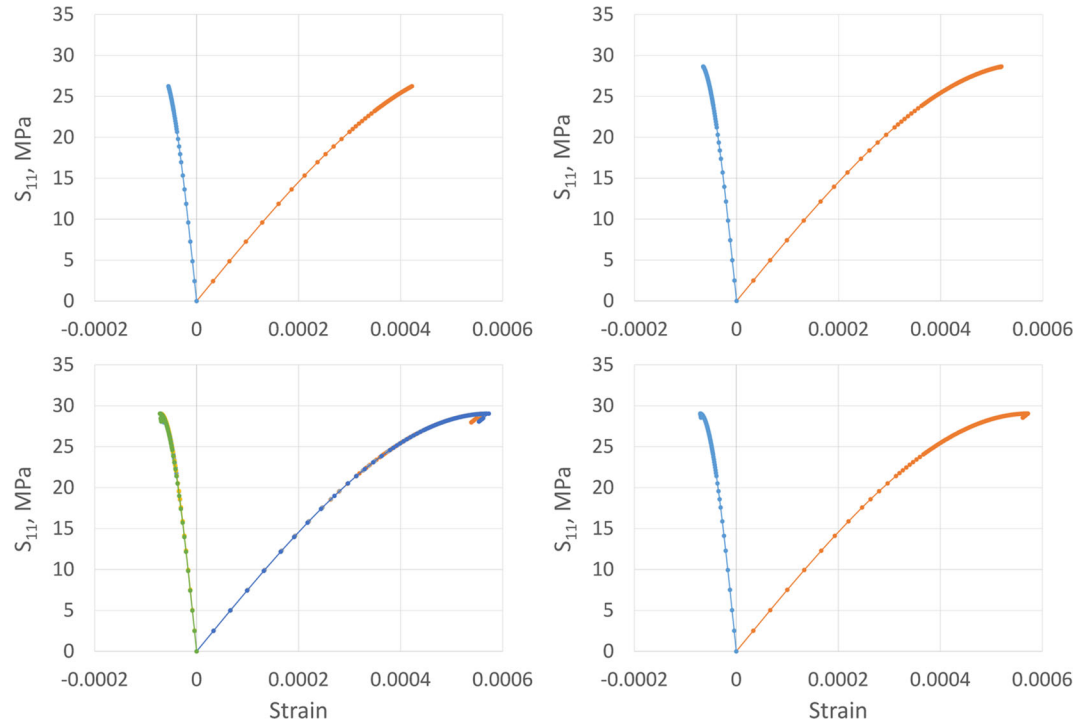

FIG. 2. S_{11} versus G_{11}^{av} (positive strain) and G_{22}^{av} (negative strain) for the tension numerical experiment. Parameters: $Y = 75$ GPa, Poisson's ratio 0.11, $k = Y$ E-6 and $n = 1$. Second gradient coefficients are set differently for each picture: in the top-left picture, the simulation has been done with a first gradient model, i.e., $\alpha_i^0 = 0.0\ Y$ $(i = 1, \ldots, 5)$; top-right: $\alpha_i^0 = 0.01\ Y$ $(i = 1, \ldots, 4)$, $\alpha_5^0 = 0.01\ Y/2$; bottom-left: $\alpha_i^0 = 0.05\ Y$ $(i = 1, \ldots, 4)$, $\alpha_5^0 = 0.05\ Y/2$; bottom-right: $\alpha_i^0 = 0.1\ Y$ $(i = 1, \ldots, 4)$, $\alpha_5^0 = 0.1\ Y/2$. In the bottom-left picture, a convergence analysis has been performed by using mesh sizes 15×10 (blue positive, green negative), 30×20 (orange positive, light blue negative, the same colors as in the other pictures of this figure) and 60×40 (gray positive, yellow negative) (color figure online)

and in the horizontal direction for the shear case,

$$f_1^{V_2} = f_1^{\text{ext},V_2} = 0, \quad f_1^{V_3} = f_1^{\text{ext},V_3} = 0. \tag{47}$$

3.2. Numerical results

We now present some numerical results obtained by solving the system of coupled PDE's on the rectangular domain ($l = 10$ mm, $L = 30$ mm) in Fig. 1 (bottom-left) (or bottom-right) with the coupled boundary conditions (40), (41), (42), (43) (or (44)), (45) and (46) (or 47). The solution algorithm will be explained in the next subsection. Of course, at time $t = 0$, the damage ω has to be initialized; we consider the *initially undamaged* case $\omega(X, 0) = 0$.

All the following simulations were performed setting the Poisson's ratio to 0.11, the resistance to damage $k = Y$ E-6, with $Y = 75$ GPa and, except for Figs. 3, 4 and 5, $n = 1$.

In Figs. 2 and 3 (or in Fig. 6), averaged stress S_{11}(or S_{12}) versus averaged strain G_{11}^{av} (positive) and G_{22}^{av} (negative) (or G_{12}^{av}) is plotted for A^0, B^0, C^0 and D^0 corresponding to those α_i^0's $(i = 1, \ldots, 5)$ made explicit in the captions. It is worth to be noted that S_{11}, G_{11}^{av} and G_{22}^{av} are all averages over the side S_3,

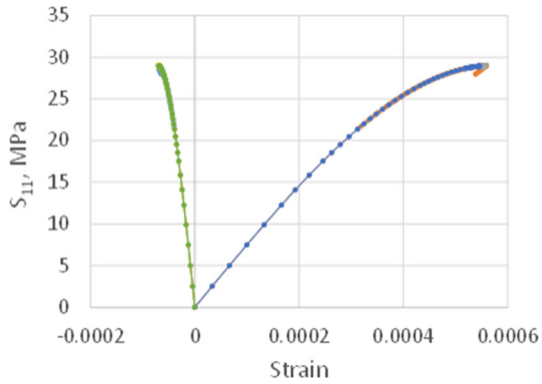

FIG. 3. S_{11} versus G_{11}^{av} (positive strain) and G_{22}^{av} (negative strain) for the tension numerical experiment. Parameters: $Y = 75$ GPa, Poisson's ratio 0.11, $k = Y$ E-6, $\alpha_i^0 = 0.05\ Y$ $(i = 1, \ldots, 4)$ and $\alpha_5^0 = 0.05\ Y/2$. Orange (light blue), gray (gray) and blue (green) positive (negative) strain correspond, respectively, to the cases $n = 1$, $n = 0$ and $n = -1$, respectively (color figure online)

which are defined as follows,

$$S_{11} = \frac{1}{2lt} \int\limits_{S_3} \sigma_{11}, \quad S_{12} = \frac{1}{2lt} \int\limits_{S_3} \sigma_{12},$$
$$G_{11}^{\mathrm{av}} = \frac{1}{2l} \int\limits_{S_3} G_{11}, \quad G_{22}^{\mathrm{av}} = \frac{1}{2l} \int\limits_{S_3} G_{22}, \quad G_{12}^{\mathrm{av}} = \frac{1}{2l} \int\limits_{S_3} G_{12}.$$

We notice that, in the top-left picture of Fig. 2, S_{11} is plotted for those values of A^0, B^0, C^0 and D^0 corresponding to $\alpha_i^0 = 0.0\ Y$ $(i = 1, \ldots, 5)$, which corresponds to the case in which the deformation energy density depends only upon the first gradient ∇u of the displacement field. We further remark that coefficients α_i^0 $(i = 1, \ldots, 5)$ change their values in the other pictures of Fig. 2, as shown in the caption. Thus, second gradient terms in the deformation energy density functional U, as far as α_i^0 $(i = 1, \ldots, 5)$ increases, increasingly acquire relative importance and significance with respect to first gradient terms. This yields in turn smoother (i.e., more regular) solutions and improved convergence of the numerical scheme. Indeed, increasing the values of α_i^0 $(i = 1, \ldots, 5)$, the average stress S_{11} can be computed for higher (smaller) values of the averaged strain G_{11}^{av} (G_{22}^{av}). We notice that, moreover, this fact unveils the emergence of a plateau in stress–strain curves, which was expected because of the stress softening behavior we have imposed in (36). Finally, for the two pictures at the bottom of Fig. 2, we observe a snap-back like transition due to elastic unloading. It is worth to be noted the this snap-back behavior is not due to any instability effect. The reason is that the stiffness reduction produces in this case an elastic unloading inducing a decreasing stress and a decreasing strain with increasing values of applied boundary displacement $\overline{u}$. In the bottom-left picture of Fig. 2 the results from different discretization density (mesh size) have been shown as described in the caption. The results with different mesh sizes virtually overlap, except for the snap-back like transition due to elastic unloading part, that could be affected by the convergence error in the Newton's iterative scheme. In Fig. 3, we show a parametrization with respect to n. In Fig. 2, we used the best regularizing effect of the case $n = 1$. In Fig. 3, the stress–strain curve is shown together with the less regularizing cases related to $n = 0$ and $n = -1$.

In this form, the results virtually overlap, except for the snap-back like transition phase, that occurs only if the second gradient elastic contribution is emphasized from damage, i.e., in the case $n = 1$. the reason is that the higher the n the smoother is the simulation. Thus, for the same reason, the farther is the ending-failure point.

Generally, we report that for the lowest values of stress the damage is relatively small and uniform throughout the domain while, for the highest values of stress (corresponding to the highest absolute values

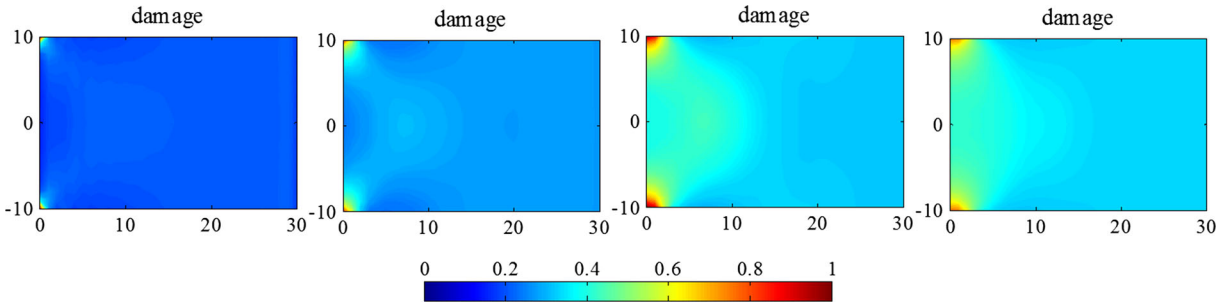

FIG. 4. Contour plot of the damage parameter ω one step before the failure, i.e., at $\overline{u} = \overline{u}_{fin}$ for the tension numerical experiment. Parameters: $Y = 75$ GPa, Poisson's ratio 0.11, $k = Y$ E-6 and $n = 1$. From the left-hand side to the right-hand side, we have an increasing value of second gradient parameters, i.e., left: $\alpha_i^0 = 0.0\ Y$ $(i = 1, \ldots, 5)$, $\overline{u}_{fin} = 13.60$ µm; center-left: $\alpha_i^0 = 0.01\ Y$ $(i = 1, \ldots, 4)$, $\alpha_5^0 = 0.01\ Y/2$, $\overline{u}_{fin} = 15.88$ µm; center-right: $\alpha_i^0 = 0.05\ Y$ $(i = 1, \ldots, 4)$, $\alpha_5^0 = 0.05\ Y/2$, $\overline{u}_{fin} = 17.56$ µm; right: $\alpha_i^0 = 0.1\ Y$ $(i = 1, \ldots, 4)$, $\alpha_5^0 = 0.1\ Y/2$, $\overline{u}_{fin} = 17.61$ µm

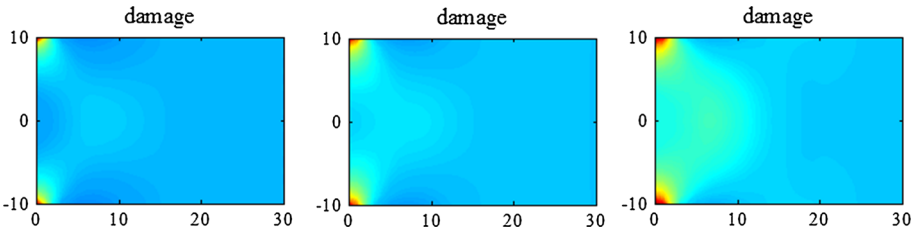

FIG. 5. Contour plot of the damage parameter ω one step before the failure for the tension numerical experiment. Parameters: $Y = 75$ GPa, Poisson's ratio 0.11, $k = Y$ E-6, $\alpha_i^0 = 0.05\ Y$ $(i = 1, \ldots, 4)$ and $\alpha_5^0 = 0.05\ Y/2$. From the left to right, we have shown, respectively, the cases corresponding to $n = -1$, $n = 0$ and $n = 1$. The scale is the same of Fig. 4

of the averaged strains G_{11}^{av} and G_{22}^{av} for which solutions are computed and shown in Fig. 4), the damage is concentrated at the left corners of the domain. We notice that the difference between the damage peaks, that are almost equal to unity since the contour plots are shown in Fig. 4 one step before the failure, at the left corners and the damage in the surrounding areas of the domain is smaller as second gradient terms in the deformation energy density gain significance. This is shown in Fig. 4, where the values of second gradient parameters increase their values from the picture at the left side to that at the right side and is coherent with the fact that the higher is the second gradient contribution, the smoother is the solution. We also remark that, for the lowest values of the second gradient parameters, two bands at 45° with respect to the axial direction propagate from the two left corners. The two bands intersect in the middle of the sample and a damaged island region appears. Moreover, for the larger values of second gradient coefficients the bands are so large that the damaged regions are no more neatly distinguishable from the rest of the sample and no island is visible at the step before failure that is shown in Fig. 4.

For the case corresponding to $\alpha_i^0 = 0.05\ Y$ $(i = 1, \ldots, 4)$ and $\alpha_5^0 = 0.05\ Y/2$, we show in Fig. 5 contour plot of the damage parameter ω, one step before the failure, for the tension numerical experiment and for different values of the parameter n, as shown in the caption. Even in this case, the two shear bands are visible only for the negative value of the parameter n. It is worth to be noted that the third contour plots of Figs. 4 and 5 are the same.

Figures 6 and 7 are the analogous, for the shear case, to Figs. 2, 3, 4 and 5. In Fig. 6, a change in the qualitative behavior of the test is visible as far as the second gradient parameters are increased. In the shear case of Fig. 6, the competition between the softening behavior and the snap-back like transition due to elastic unloading is more evident. Even in this case, it is worth to be noted the this snap-back

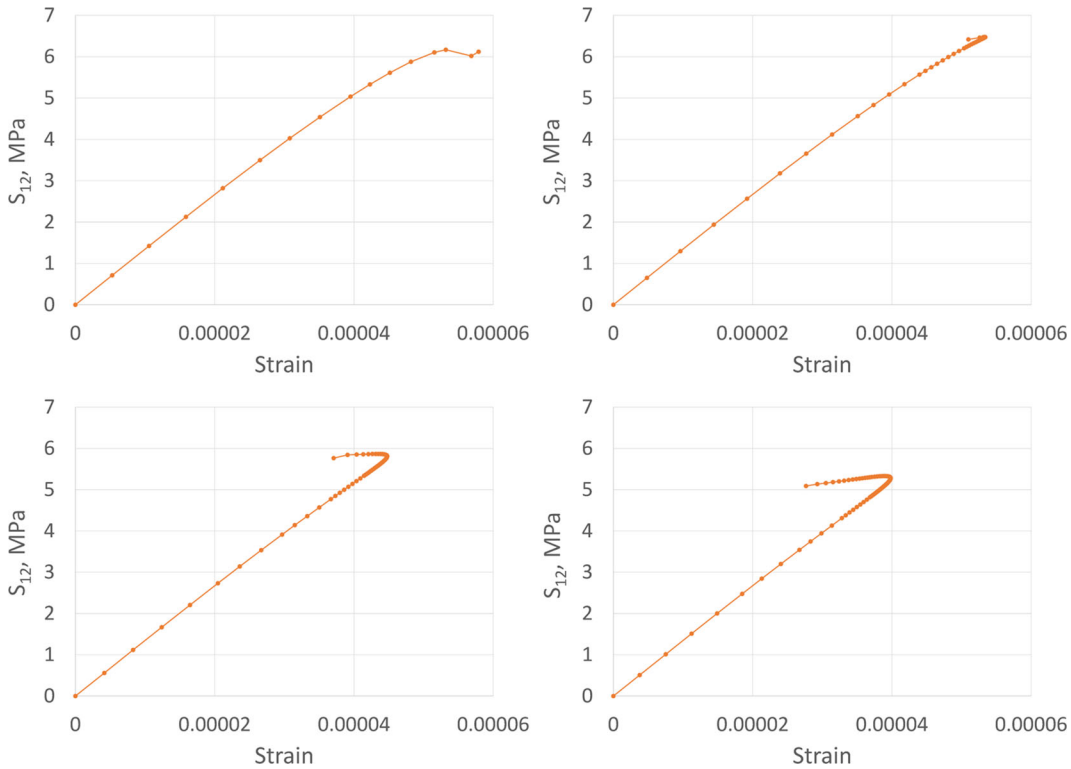

FIG. 6. S_{12} versus G_{12}^{av} for the shear numerical experiment. Parameters: $Y = 75$ GPa, Poisson's ratio 0.11, $k = Y$ E-6 and $n = 1$. Second gradient coefficients are set differently for each picture: In the top-left picture, the simulation has been performed with a first gradient model, i.e., $\alpha_i^0 = 0.0\ Y$ $(i = 1, \ldots, 5)$; top-right: $\alpha_i^0 = 0.01\ Y$ $(i = 1, \ldots, 4)$, $\alpha_5^0 = 0.01\ Y/2$; bottom-left: $\alpha_i^0 = 0.05\ Y$ $(i = 1, \ldots, 4)$, $\alpha_5^0 = 0.05\ Y/2$; bottom-right: $\alpha_i^0 = 0.1\ Y$ $(i = 1, \ldots, 4)$, $\alpha_5^0 = 0.1\ Y/2$

behavior is not due to any instability effect. The reason again is that the stiffness reduction produces an elastic unloading inducing a decreasing stress and a decreasing strain with increasing values of applied boundary displacement $\overline{v}$.

In Fig. 7 ,contour plots of the damage parameter, in the shear case, are shown. The same comments on the relevance of the second gradient coefficients can be done, even though no shear bands are being observed.

3.3. Solution algorithm

The model is new and clearly there are no available commercial finite element solvers for it. Moreover, also the implementation of KKT conditions in those solvers able to manage higher-order gradient models is not standard. For these reasons, an in-house code based on element-free Galerkin (EFG) method has been employed for our numerical calculations [10,45]. In the EFG method, the domain is discretized into a set of nodes and moving least square (MLS) shape functions are used as the trail and the test functions. For the 2D case, the MLS approximation is expressed as

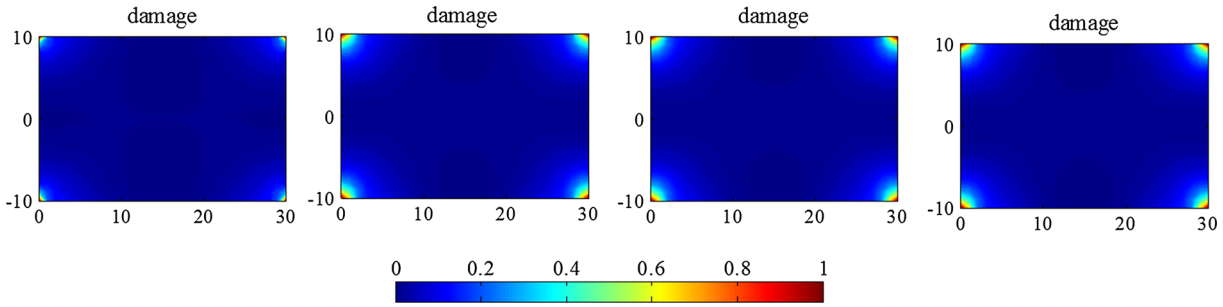

FIG. 7. Contour plot of the damage parameter ω one step before the failure, i.e., at $\overline{v} = \overline{v}_{fin}$ for the shear numerical experiment. Parameters: $Y = 75$ GPa, Poisson's ratio 0.11, $k = Y$ E-6 and $n = 1$. From the left to the right, we have an increasing value of second gradient parameters, i.e., left: $\alpha_i^0 = 0.0\ Y$ $(i = 1, \ldots, 5)$, $\overline{v}_{fin} = 10.0\,\mu$m; center-left: $\alpha_i^0 = 0.01\ Y$ $(i = 1, \ldots, 4)$, $\alpha_5^0 = 0.01\ ^Y/_2$, $\overline{v}_{fin} = 12.6\ \mu$m; center-right: $\alpha_i^0 = 0.05\ Y$ $(i = 1, \ldots, 4)$, $\alpha_5^0 = 0.05\ ^Y/_2$, $\overline{v}_{fin} = 14.4\ \mu$m; right: $\alpha_i^0 = 0.1\ Y$ $(i = 1, \ldots, 4)$, $\alpha_5^0 = 0.1\ ^Y/_2$, $\overline{v}_{fin} = 15.3\ \mu$m

$$\{u\}_{2\times 1} = [\Phi]^T_{2\times 2n}\,\{U_s\}_{2n\times 1} \tag{48}$$

where U_s is the vector collecting the nodal displacements within the influence domain, and $\Phi^T(x)$ is the matrix of MLS shape functions corresponding to n nodes in the influence domain of the sampling point x, written as

$$[\Phi]^T_{2\times 2n} = [p]^T_{2\times 2n}\,[A]^{-1}_{12\times 12}\,[B]_{12\times 2n}\,. \tag{49}$$

The matrix p is formed of the monomial terms of the quadratic basis as

$$[p]^T_{2\times 12} = \begin{bmatrix} 1 & x & y & x^2 & xy & y^2 & 0 & 0 & 0 & 0 & 0 & 0 \\ 0 & 0 & 0 & 0 & 0 & 0 & 1 & x & y & x^2 & xy & y^2 \end{bmatrix} \tag{50}$$

and the matrix A and vector B are given as

$$[A]_{12\times 12} = \left[\sum_{i=1}^{n} w_i\,(x,y)\,[p\,(x_i,y_i)]_{12\times 2}\,[p\,(x_i,y_i)]^T_{2\times 12}\right] \tag{51}$$

$$[B]_{12\times 2n} = \begin{bmatrix} w_1\,(x,y)\,[p\,(x_1,y_1)]_{12\times 2} & w_2\,(x,y)\,[p\,(x_2,y_2)]_{12\times 2} & \cdots \\ \cdots & w_n\,(x,y)\,[p\,(x_n,y_n)]_{12\times 2} \end{bmatrix}. \tag{52}$$

The weight functions $w_i(x,y)$ are specified as the product of 1D cubic splines in the x- and y- directions

$$w_i(x,y) = w_{ix}(x) w_{iy}(y). \tag{53}$$

The x-direction cubic spline is given as (and the y-direction cubic spline is similarly defined)

$$w_{ix}(x,y) = \begin{cases} \frac{2}{3} - 4\overline{r}_{ix}^2 + 4\overline{r}_{ix}^3 & \overline{r}_{ix} \le 0.5 \\ \frac{4}{3} - 4\overline{r}_{ix} + 4\overline{r}_{ix}^2 - \frac{4}{3}\overline{r}_{ix}^3 & 0.5 < \overline{r}_{ix} \le 1 \\ 0 & \overline{r}_{ix} \ge 1 \end{cases} \tag{54}$$

where $\overline{r}_{ix} = \frac{|x - x_i|}{d_{sx}}$, $|x - x_i|$ is the distance from node x_i to the sampling point x and the x-dimension of the rectangular influence domain $d_{sx} = \beta d_{cx}$ (with $\beta = 3$) in which d_{cx} is the x-nodal spacing.

Substituting Eq. (48) into the weak form of the partial differential equations will result in the following system of algebraic equations [77,78]

$$\left[K_{ps} + \overline{K}_{ps}\right]\{U_s\} = \left\{F_p + \overline{F}_p\right\}. \tag{55}$$

In Eq. (55), the terms with bar arise from the penalty method used to implement the displacement boundary conditions. The stiffness matrices K_{ps}, $\overline{K}_{ps}$ and the force vectors F_p, $\overline{F}_p$ are given as

$$[K_{ps}]_{2n\times 2n} = \int_{\mathcal{B}} [\partial\Phi]_{2n\times 3}\,(1-\omega)\,[D]_{3\times 3}\,[\partial\Phi]^T_{3\times 2n} \tag{56}$$
$$+ \left[\partial^2\Phi\right]_{2n\times 8}\,(1+n\omega)\,[\underline{D}]_{8\times 8}\,\left[\partial^2\Phi\right]^T_{8\times 2n}$$
$$\left[\overline{K}_{ps}\right]_{2n\times 2n} = -\int_{\partial\mathcal{B}} \alpha\,[\Phi]_{2n\times 2}\,[\Phi]^T_{2\times 2n} \tag{57}$$
$$\{F_p\}_{2n\times 1} = \int_{\partial\mathcal{B}} [\Phi]_{2n\times 2}\,\{t\}_{2\times 1} + [\partial\Phi]_{2n\times 3}\,[n]_{3\times 2}\,\{\tau\}_{2\times 1} \tag{58}$$
$$+ \int_{\partial\partial\mathcal{B}} [\Phi]_{2n\times 2}\,\{f\}_{2\times 1}$$
$$\left\{\overline{F}_p\right\}_{2n\times 1} = -\int_{\partial\mathcal{B}} \alpha\,[\Phi]_{2n\times 2}\,[\overline{u}]_{2\times 1}\,. \tag{59}$$

In Eq. (56), the elasticity matrices $[D]$ and $[\underline{D}]$ are obtained from Eq. (33) and the expression for ω is given in Eq. (39). The penalty parameter, α, is determined as 10^6 times the maximum diagonal element of the elastic global stiffness matrix. Clearly, the obtained algebraic system in Eq. (55) is nonlinear and it is solved using Newton's approach. The efficiency of the present method has been shown in the bottom-left picture of Fig. 2, where the result has been shown from different discretization density (mesh size). We remark that in element-free Galerkin scheme we are using, we do not have a mesh in same sense as Finite Element.

4. Summary and conclusions

A variational formulation of damage mechanics in the case of linear elastic second gradient isotropic continua in the small deformation context has been developed. In the presented approach, the total deformation energy functional is taken to depend not only upon the displacement field but also upon the damage field. Since damage represents an irreversible phenomenon, a non-standard variational principle is proposed which, remarkably, leads to the so-called Karush–Kuhn–Tucker (KKT) optimality conditions for damage evolution. The developed variational procedure is particularized for the 2D case and an expression for the energy density functional, accounting for damage, is provided. For the 2D case, the constitutive parameters are selected along with the relevant conditions for positive definiteness of the energy density function. A more reliable identification procedure [36,63,64] still needs to be implemented. The governing PDE's and the explicit expression for damage evolution are derived. Boundary conditions are identified and expounded through two particular examples of a plate subjected to in-plane external loadings. The examples clearly illustrate the relevant boundary conditions for the second gradient continua, particularly with respect to the conditions associated with boundary gradients and vertices at boundary intersections. Finally, we present numerical simulations to illustrate the applicability of the derived formulation.

The simulation results show that as the second gradient terms increase in significance, the achieved solution is smoother. In particular, we have shown that the case $n > 0$ increases the stability of the simulations with respect to the case $n < 0$ and it is compatible, in the analyzed case, with the snap-back like transition phase due to the elastic unloading effect (see Fig. 3). In addition, in Fig. 5 we have shown that for $n < 0$ the reduction of the characteristic length induces a more clear strain localization. Clearly,

the sign of the parameter n cannot be deduced by any physical or abstract principle, but it should be determined from experimental measurements.

Indeed, it is remarkable that very little attention has been paid in the literature to the case of diffused damage ($n > 0$) which results in further microstructural development and increase in second gradient parameters while the material experiences an overall softening. Such a case of material behavior has been widely ignored in favor of the traditional case of localizing damage and fracture. To this end, the damage model derived in the present work could serve as an impetus for experimentalists to reassess measured outcomes of material damage from a general viewpoint, particularly in disordered material systems for which there are no adscititious conditions for development of localization. It is in fact intriguing to consider the case of $n > 0$ material when the damage ω reaches 1, such that the material is now reduced to a purely second gradient material characterized by many internal floppy modes. Such materials are not beyond the realm of imagination (or reality) [1]. In this sense, the presented work represents a first, albeit significant, step toward a broader damage theory.

It is interesting to observe that the damage, in these systems, initiates at the boundary due to the peculiar boundary conditions. Such boundary effects have implications upon interpretation of experimental measurements, wherein the results could be affected by the ability to precisely control boundary conditions or the interactions of the boundary conditions with intrinsic material defects. The presented second gradient continuum approach is attractive since it has the ability to consider the effects of the underlying microscale damage mechanism that are typically beyond reach of the available approaches. Furthermore, the variational approach developed in this work allows us to recover not only the relevant governing equations and the damage evolution relationship but also unambiguous boundary conditions.

Acknowledgements

This work was supported by a grant from the Government of the Russian Federation (Contract No. 14.Y26.31.0031). AM is also supported by the National Science Foundation (NSF) under CMMI-1727433.

References

[1] Alibert, J.-J., Seppecher, P., dell'Isola, F.: Truss modular beams with deformation energy depending on higher displacement gradients. Math. Mech. Solids **8**(1), 51–73 (2003)
[2] Altenbach, H., Eremeyev, V.: On the linear theory of micropolar plates. J. Appl. Math. Mech. Zeitschrift für Angewandte Mathematik und Mechanik (ZAMM) **89**(4), 242–256 (2009)
[3] Ambrosio, L., Tortorelli, V.M.: Approximation of functional depending on jumps by elliptic functional via t-convergence. Commun. Pure Appl. Math. **43**(8), 999–1036 (1990)
[4] AminPour, H., Rizzi, N.: A one-dimensional continuum with microstructure for single-wall carbon nanotubes bifurcation analysis. Math. Mech. Solids **21**(2), 168–181 (2016)
[5] Amor, H., Marigo, J.-J., Maurini, C.: Reguralized formulation of the variational brittle fracture with unilateral contact: numerical experiment. J. Mech. Phys. Solids **57**, 1209–1229 (2009)
[6] Andreaus, U., Giorgio, I., Lekszycki, T.: A 2D continuum model of a mixture of bone tissue and bio-resorbable material for simulating mass density redistribution under load slowly variable in time. Zeitschrift für Angewandte Mathematik und Mechanik **13**, 7 (2013)
[7] Andreaus, U., Giorgio, I., Madeo, A.: Modeling of the interaction between bone tissue and resorbable biomaterial as linear elastic materials with voids. Zeitschrift für angewandte Mathematik und Physik **66**(1), 209–237 (2014)
[8] Aslan, O., Forest, S.: The micromorphic versus phase field approach to gradient plasticity and damage with application to cracking in metal single crystals. In: Multiscale Methods in Computational Mechanics, pp. 135–153. Springer (2011)
[9] Auffray, N., dell'Isola, F., Eremeyev, V., Madeo, A., Rosi, G.: Analytical continuum mechanics à la Hamilton–Piola least action principle for second gradient continua and capillary fluids. Math. Mech. Solids **20**(4), 375–417 (2015)
[10] Belytschko, T., Lu, Y.Y., Gu, L.: Element-free Galerkin methods. Int. J. Numer. Methods Eng. **37**(2), 229–256 (1994)
[11] Bilotta, A., Formica, G., Turco, E.: Performance of a high-continuity finite element in three-dimensional elasticity. Int. J. Numer. Methods Biomed. Eng. **26**(9), 1155–1175 (2010)

[12] Bourdin, B., Francfort, G.A., Marigo, J.-J.: The variational approach to fracture. J. Elast. **91**, 5–148 (2008)
[13] Carcaterra, A., Akay, A., Bernardini, C.: Trapping of vibration energy into a set of resonators: theory and application to aerospace structures. Mech. Syst. Signal Process. **26**, 1–14 (2012)
[14] Carcaterra, A., dell'Isola, F., Esposito, R., Pulvirenti, M.: Macroscopic description of microscopically strongly inhomogenous systems: a mathematical basis for the synthesis of higher gradients metamaterials. Arch. Ration. Mech. Anal. **218**(3), 1239–1262 (2015)
[15] Cazzani, A., Malagù, M., Turco, E.: Isogeometric analysis: a powerful numerical tool for the elastic analysis of historical masonry arches. Contin. Mech. Thermodyn. **28**(1–2), 139–156 (2016)
[16] Cazzani, A., Stochino, F., Turco, E.: An analytical assessment of finite element and isogeometric analyses of the whole spectrum of Timoshenko beams. J. Appl. Math. Mech. Zeitschrift für Angewandte Mathematik und Mechanik (ZAMM) **96**(10), 1220–1244 (2016)
[17] Cecchi, A., Rizzi, N.: Heterogeneous elastic solids: a mixed homogenization-rigidification technique. Int. J. Solids Struct. **38**(1), 29–36 (2001)
[18] Chen, J., Ouyang, L., Rulis, P., Misra, A., Ching, W.Y.: Complex nonlinear deformation of nanometer intergranular glassy films in β-Si_3N_4. Phys. Rev. Lett. **95**(256103), 25 (2005)
[19] Contrafatto, L., Cuomo, M., Fazio, F.: An enriched finite element for crack opening and rebar slip in reinforced concrete members. Int. J. Fract. **178**(1–2), 33–50 (2012)
[20] Contrafatto, L., Cuomo, M., Gazzo, S.: A concrete homogenisation technique at meso-scale level accounting for damaging behaviour of cement paste and aggregates. Comput. Struct. **173**, 1–18 (2016)
[21] Contrafatto, L., Cuomo, M., Greco, L.: Meso-scale simulation of concrete multiaxial behaviour. Eur. J. Environ. Civ. Eng. **21**(7–8), 896–911 (2017)
[22] Cuomo, M., Contrafatto, L., Greco, L.: A variational model based on isogeometric interpolation for the analysis of cracked bodies. Int. J. Eng. Sci. **80**, 173–188 (2014)
[23] de Felice, G., Rizzi, N.: Macroscopic modelling of cosserat media. Trends Appl. Math. Mech. Monogr. Surv. Pure Appl. Math. **106**, 58–65 (1999)
[24] dell'Isola, F., d'Agostino, M., Madeo, A., Boisse, P., Steigmann, D.: Minimization of shear energy in two dimensional continua with two orthogonal families of inextensible fibers: the case of standard bias extension test. J. Elast. **122**(2), 131–155 (2016)
[25] dell'Isola, F., Della Corte, A., Giorgio, I.: Higher-gradient continua: the legacy of piola, mindlin, sedov and toupin and some future research perspectives. Math. Mech. Solids **22**(4), 1–21 (2017)
[26] dell'Isola, F., Della Corte, A., Greco, L., Luongo, A.: Plane bias extension test for a continuum with two inextensible families of fibers: a variational treatment with lagrange multipliers and a perturbation solution. Int. J. Solids Struct. **81**, 1–12 (2016)
[27] dell'Isola, F., Giorgio, I., Andreaus, U.: Elastic pantographic 2D lattices: a numerical analysis on static response and wave propagation. Proc. Est. Acad. Sci. **64**, 219–225 (2015)
[28] dell'Isola, F., Giorgio, I., Pawlikowski, M., Rizzi, N.: Large deformations of planar extensible beams and pantographic lattices: heuristic homogenization, experimental and numerical examples of equilibrium. In: Proc. R. Soc. A, vol. 472, p. 20150790. The Royal Society (2016)
[29] dell'Isola, F., Placidi, L.: Variational principles are a powerful tool also for formulating field theories. In: Variational Models and Methods in Solid and Fluid Mechanics, pp. 1–15. Springer (2011)
[30] dell'Isola, F., Seppecher, P., Della Corte, A.: The postulations á la D'Alembert and á la Cauchy for higher gradient continuum theories are equivalent: a review of existing results. In: Proc. R. Soc. A, vol. 471, p. 20150415. The Royal Society (2015)
[31] dell'Isola, F., Steigmann, D.J.: A two-dimensional gradient-elasticity theory for woven fabrics. J. Elast. **18**, 113–125 (2015)
[32] Di Carlo, A., Rizzi, N., Tatone, A.: Continuum modelling of a beam-like latticed truss: identification of the constitutive functions for the contact and inertial actions. Meccanica **25**(3), 168–174 (1990)
[33] Duda, F.P., Ciarbonetti, A., Sánchez, P.J., Huespe, A.E.: A phase-field/gradient damage model for brittle fracture in elastic–plastic solids. Int. J. Plast. **65**, 269–296 (2015)
[34] Ferretti, M., Madeo, A., dell'Isola, F., Boisse, P.: Modeling the onset of shear boundary layers in fibrous composite reinforcements by second-gradient theory. Zeitschrift für angewandte Mathematik und Physik **65**(3), 587–612 (2014)
[35] Forest, S.: Micromorphic approach for gradient elasticity, viscoplasticity, and damage. J. Eng. Mech. **135**(3), 117–131 (2009)
[36] Giorgio, I.: Numerical identification procedure between a micro-cauchy model and a macro-second gradient model for planar pantographic structures. Zeitschrift für angewandte Mathematik und Physik **67**(4), 95 (2016)
[37] Giorgio, I., Andreaus, U., Lekszycki, T., Della Corte, A.: The influence of different geometries of matrix/scaffold on the remodeling process of a bone and bioresorbable material mixture with voids. Math. Mech. Solids **22**(5), 969–987 (2017)
[38] Giorgio, I., Grygoruk, R., dell'Isola, F., Steigmann, D.J.: Pattern formation in the three-dimensional deformations of fibered sheets. Mech. Res. Commun. **69**, 164–171 (2015)

[39] Goda, I., Assidi, M., Ganghoffer, J.F.: A 3D elastic micropolar model of vertebral trabecular bone from lattice homogenization of the bone microstructure. Biomech. Model. Mechanobiol. **13**, 53–83 (2014)
[40] Greco, L., Cuomo, M.: B-spline interpolation of Kirchhoff-Love space rods. Comput. Methods Appl. Mech. Eng. **256**, 251–269 (2013)
[41] Greco, L., Cuomo, M.: An implicit G1 multi patch B-spline interpolation for Kirchhoff-Love space rod. Comput. Methods Appl. Mech. Eng. **269**, 173–197 (2014)
[42] Grillo, A., Wittum, G., Tomic, A., Federico, S.: Remodelling in statistically oriented fibre-reinforced composites and biological tissues. Math. Mech. Solids **20**, 1107–1129 (2015)
[43] Harrison, P.: Modelling the forming mechanics of engineering fabrics using a mutually constrained pantographic beam and membrane mesh. Compos. A Appl. Sci. Manuf. **81**, 145–157 (2016)
[44] Harrison, P., Clifford, M.J., Long, A.C.: Shear characterisation of viscous woven textile composites: a comparison between picture frame and bias extension experiments. Compos. Sci. Technol. **64**(10), 1453–1465 (2004)
[45] Liu, G.-R., Gu, Y.-T.: An Introduction to Meshfree Methods and Their Programming. Springer, Berlin (2005)
[46] Lorentz, E., Andrieux, S.: Analysis of non-local models through energetic formulations. Int. J. Solids Struct. **40**(12), 2905–2936 (2003)
[47] Mindlin, R.D.: Micro-structure in linear elasticity. Arch. Ration. Mech. Anal. **16**, 51–78 (1964)
[48] Misra, A., Ouyang, L., Chen, J., Ching, W.Y.: Ab initio calculations of strain fields and failure patterns in silicon nitride intergranular glassy films. Philos. Mag. **87**(25), 3839–3852 (2007)
[49] Misra, A., Poorsolhjouy, P.: Granular micromechanics model for damage and plasticity of cementitious materials based upon thermomechanics. Math. Mech. Solids (2015). https://doi.org/10.1177/1081286515576821
[50] Misra, A., Poorsolhjouy, P.: Granular micromechanics based micromorphic model predicts frequency band gaps. Contin. Mech. Thermodyn. **28**(1–2), 215–234 (2016)
[51] Misra, A., Poorsolhjouy, P.: Granular micromechanics model of anisotropic elasticity derived from Gibbs potential. Acta Mech. **227**(5), 1393–1413 (2016)
[52] Misra, A., Singh, V.: Micromechanical model for viscoelastic materials undergoing damage. Contin. Mech. Thermodyn. **25**(2–4), 343–358 (2013)
[53] Misra, A., Singh, V.: Thermomechanics-based nonlinear rate-dependent coupled damage-plasticity granular micromechanics model. Contin. Mech. Thermodyn. **27**(4–5), 787–817 (2015)
[54] Peerlings, R.H.J., Geers, M.G.D., De Borst, R., Brekelmans, W.A.M.: A critical comparison of nonlocal and gradient-enhanced softening continua. Int. J. Solids Struct. **38**(44), 7723–7746 (2001)
[55] Pham, K., Marigo, J.-J.: Approche variationnelle de l'endommagement: I. les concepts fondamentaux. C.R. Mécanique **338**, 191–198 (2010)
[56] Pham, K., Marigo, J.-J.: Approche variationnelle de l'endommagement: II. les modèles à gradient. C.R. Mécanique **338**, 199–206 (2010)
[57] Pham, K., Marigo, J.-J.: From the onset of damage to rupture: construction of responses with damage localization for a general class of gradient damage models. Contin. Mech. Thermodyn. **25**(2–4), 147–171 (2013)
[58] Pham, K., Marigo, J.-J., Maurini, C.: The issue of the uniqueness and the stability of the homogeneous response in uniaxial tests with gradient damage models. J. Mech. Phys. Solids **59**, 1163–1190 (2011)
[59] Piccardo, G., Ranzi, G., Luongo, A.: A complete dynamic approach to the generalized beam theory cross-section analysis including extension and shear modes. Math. Mech. Solids **19**, 900–924 (2014)
[60] Pietraszkiewicz, W., Eremeyev, V.: On natural strain measures of the non-linear micropolar continuum. Int. J. Solids Struct. **46**(3), 774–787 (2009)
[61] Placidi, L.: A variational approach for a nonlinear 1-dimensional second gradient continuum damage model. Contin. Mech. Thermodyn. **27**(4–5), 623–638 (2015)
[62] Placidi, L.: A variational approach for a nonlinear one-dimensional damage-elasto-plastic second-gradient continuum model. Contin. Mech. Thermodyn. **28**(1–2), 119–137 (2016)
[63] Placidi, L., Andreaus, U., Della Corte, A., Lekszycki, T.: Gedanken experiments for the determination of two-dimensional linear second gradient elasticity coefficients. Zeitschrift für angewandte Mathematik und Physik **66**(6), 3699–3725 (2015)
[64] Placidi, L., Andreaus, U., Giorgio, I.: Identification of two-dimensional pantographic structure via a linear D4 orthotropic second gradient elastic model. J. Eng. Math. (2017). https://doi.org/10.1007/s10665-016-9856-8:1-21
[65] Placidi, L., Barchiesi, E.: Energy approach to brittle fracture in strain gradient modelling. Proc. R. Soc. Math. Phys. Eng. Sci. **474**, 20170878 (2018)
[66] Placidi, L., El Dhaba, A.: Semi-inverse method à la saint-venant for two-dimensional linear isotropic homogeneous second-gradient elasticity. Math. Mech. Solids **22**(5), 919–937 (2017)
[67] Placidi, L., Greco, L., Bucci, S., Turco, E., Rizzi, N.L.: A second gradient formulation for a 2D fabric sheet with inextensible fibres. Zeitschrift für angewandte Mathematik und Physik **67**(5), 114 (2016)
[68] Placidi, L., Greve, R., Seddik, H., Faria, S.: Continuum-mechanical, anisotropic flow model for polar ice masses, based on an anisotropic flow enhancement factor. Contin. Mech. Thermodyn. **22**(3), 221–237 (2010)

[69] Placidi, L., Hutter, K.: Thermodynamics of polycrystalline materials treated by the theory of mixtures with continuous diversity. Contin. Mech. Thermodyn. **17**(6), 409–451 (2006)
[70] Poorsolhjouy, P., Misra, A.: Effect of intermediate principal stress and loading-path on failure of cementitious materials using granular micromechanics. Int. J. Solids Struct. **108**, 139–152 (2017)
[71] Rinaldi, A., Placidi, L.: A microscale second gradient approximation of the damage parameter of quasi-brittle heterogeneous lattices. J. Appl. Math. Mech. Zeitschrift für Angewandte Mathematik und Mechanik (ZAMM) **94**(10), 862–877 (2014)
[72] Scerrato, D., Giorgio, I., Rizzi, N.: Three-dimensional instabilities of pantographic sheets with parabolic lattices: numerical investigations. Zeitschrift für angewandte Mathematik und Physik **67**(3), 1–19 (2016)
[73] Scerrato, D., Zhurba Eremeeva, I.A., Lekszycki, T., Rizzi, N.L.: On the effect of shear stiffness on the plane deformation of linear second gradient pantographic sheets. J. Appl. Math. Mech. Zeitschrift für Angewandte Mathematik und Mechanik (ZAMM) **96**(11), 1268–1279 (2016)
[74] Seddik, H., Greve, R., Placidi, L., Hamann, I., Gagliardini, O.: Application of a continuum-mechanical model for the flow of anisotropic polar ice to the EDML core, Antarctica. J. Glaciol. **54**(187), 631–642 (2008)
[75] Sicsic, P., Marigo, J.-J.: From gradient damage laws to Griffith's theory of crack propagation. J. Elast. **113**(1), 55–74 (2013)
[76] Voyiadjis, G.Z., Mozaffari, N.: Nonlocal damage model using the phase field method: theory and applications. Int. J. Solids Struct. **50**(20), 3136–3151 (2013)
[77] Yang, Y., Ching, W.Y., Misra, A.: Higher-order continuum theory applied to fracture simulation of nanoscale intergranular glassy film. J. Nanomech. Micromech. **1**(2), 60–71 (2011)
[78] Yang, Y., Misra, A.: Micromechanics based second gradient continuum theory for shear band modeling in cohesive granular materials following damage elasticity. Int. J. Solids Struct. **49**(18), 2500–2514 (2012)

Luca Placidi
Faculty of Engineering
International Telematic University Uninettuno
C.so Vittorio Emanuele II, 39
00186 Rome
Italy
e-mail: luca.placidi@uninettunouniversity.net

Anil Misra
Civil, Environmental and Architectural Engineering Department
The University of Kansas
1530 W. 15th Street
Lawrence KS 66045-7609
USA

Emilio Barchiesi
Dipartimento di Ingegneria Strutturale e Geotecnica
Università degli Studi di Roma "La Sapienza"
Via Eudossiana, 18
00184 Rome
Italy

(Received: January 15, 2018; revised: March 28, 2018)